ULTRA-LOW NOISE, HIGH-SENSITIVITY MEMS ACCELEROMETER FOR SATELLITE GRAVIMETRY

Inês S. Garcia[1 2], Abdelrahman M. Elhawash[1], Jorge Cabral[2], Tiago Hormigo[3], João T. da Encarnação[4,5], Filipe S. Alves[1,2] and Rosana A. Dias[1]*
[1]International Iberian Nanotechnology Laboratory (INL), 4715-330 Braga, Portugal
[2]ALGORITMI Center, University of Minho, Campus Azurém, 4800-058 Guimarães, Portugal
[3]Spin.Works S.A., Portugal
[4]Delft University of Technology, Netherlands
[5]Center for Space Research, The University of Texas at Austin, USA

ABSTRACT

Satellite gravimetry requires sub-ng acceleration measurement at frequencies below 100mHz. To bring the performance of a MEMS accelerometer closer to this level, one must decrease noise sources and maximize sensitivity (to decrease input-referred electronic noise). Electrostatic pull-in based operation has great potential for high sensitivity since it relies on time transduction. Devices were fabricated with maximized proof mass (170mg over a 13x14mm2 footprint) and tuned damping coefficient (trade-off between noise and sensitivity – pull-in operation requires low Q-factors). Novel stopper designs and caps limit both in-plane and out-of-plane displacements. Devices tested using pull-in voltage-based transduction showed sensitivity of 218 V/g.

KEYWORDS

MEMS accelerometer, pull-in time, gravimetry, ultra-low noise, high-sensitivity

INTRODUCTION

The Earth has been suffering several climatic changes in the past few years that can drastically affect how we live. It is necessary to understand the progress of climatic change and how the various geophysical processes are interconnected, and satellite gravimetry has been shown to be valuable tool over the past few years since it allows to measure mass changes at the Earth's surface. Missions such as CHAMP (DLR), GRACE (DLR / NASA) and GOCE (ESA) have already offered solutions to this challenge, with high development and operational costs [1]. The accelerometer developed for the GRACE-FO mission, on the most sensitive axes, presented a noise spectral density below 0.1nm/s^2/√Hz in the range 10mHz to 1Hz [2]and below 1nm/s^2/√Hz at 0.1mHz.

In order to enable gravimetric missions using miniaturized satellites, geodetic-grade accelerometers with a small size, reduced power consumption and low fabrication costs are required. However, gravimetry and seismology applications require accelerometers with very demanding sensitivity, noise and low frequency specifications, capable of sub-ng acceleration measurements at frequencies below 100mHz.

MEMS devices have reached noise levels of 2.5nm/s^2/√Hz at frequencies below 1Hz [3], while conventional gravimeters can display similar performance even at 10mHz [4]. In electrostatically actuated parallel-plate MEMS structures, the pull-in transition can be explored as a transduction mechanism by applying a voltage higher than the pull-in voltage while measuring the time between the start of the actuation and the pull-in displacement detection [5].

The aim of this work is to develop a geodetic-grade 1-DOF MEMS accelerometer based on pull-in time transduction. A microstructure was therefore designed to maximize the sensitivity limits of this technology and minimize the Brownian noise.

PULL-IN TIME-BASED ACCELEROMETER

Working principle

A pull-in time-based MEMS accelerometer [6] uses electrostatically actuated parallel-plate microstructures that are constantly driven to pull-in. This requires that an actuation voltage higher than the threshold pull-in voltage, V_{PI}, is applied between the parallel-plates. This voltage generates an attraction force between the movable and the anchored plates. The nominal (in case no acceleration is applied) pull-in voltage is determined using (1), here d_0 is the initial distance between the parallel-plates, C_0 the rest capacitance and k the elastic spring constant [6]:

$$V_{PI} = \sqrt{\frac{8}{27}\frac{d_0^2 k}{C_0}} \tag{1}$$

The threshold pull-in voltage also depends on acceleration, according to (2) where m is the proof mass and a is the external acceleration.

$$V_{PI,a} = \sqrt{\frac{8}{27}\frac{(d_0 - ma/k)^2\, k}{C_0}} \tag{2}$$

While the microstructure is actuated to pull-in, a set of sensing electrodes is used to measure (capacitively) the movable mass displacement and this signal is used to detect a chosen displacement threshold corresponding to near full-gap displacement (comprising therefore the full pull-in transition).

Under certain actuation and damping conditions, the pull-in transition shows a highly nonlinear profile of displacement over time, including a plateau at the critical pull-in deflection (1/3 d_0), the so-called meta-stable region. The existence of this region renders the pull-in displacement, and the corresponding pull-in time very sensitive to external accelerations. The pull-in time is measured/counted from the start of the actuation (the moment when a step voltage applied, $V_{STEP}=\alpha V_{PI}$, where $1<\alpha\approx 1$) until the proof-mass reaches a displacement well beyond the critical deflection, usually set between 80 and 95% of the full gap. This approach allows very high acceleration resolution since a time measurement is performed instead of a direct transduction of capacitance into acceleration. Moreover, differential measurements are used to improve linearity as well thermal compensation.

The sensitivity of a pull-in time accelerometer, closely related to the metastable region, depends on the actuation voltage (should be just slightly higher than the nominal pull-in voltage) and on the damping conditions – microstructures must present sufficient damping (b) since underdamped or high Q (quality factor) microstructures do not present metastability. The damper design is therefore critical since a trade-off must be met between maximizing sensitivity (b increase) and decreasing thermomechanical noise (b decrease) [6].

Designed Structures

In order to maximize acceleration sensitivity, the MEMS design focused on increasing both spring compliance and proof-mass for a maximum footprint of 13mm by 14mm, cf.in Figure 1, while tuning the damping coefficient.

The highly compliant springs have been achieved by exploring fabrication limits (at the limit between manufacturability/yield and compliance maximization), resulting in a design with six folded-springs suspending the large proof-mass (170mg, obtained by leaving a portion of the handle wafer attached to the movable structures).

Since devices with low-quality factors (between 0.5 and 2 – underdamped but near the critically damped condition) are targeted and the proof masses are quite large, it was necessary to increase the number of dampers. The squeeze-film damping is the main damping source, established in gap-changing parallel-plates. Dummy dampers have been previously implemented on the SOI handle wafer [5] but it was found that the damping coefficient achieved per unit of designed area is higher when implemented in the device layer dampers given the higher aspect ratios achievable.

In Table 1, the main design parameters of the intended devices are presented: two different types of devices have been designed, differing in the number of dampers.

Besides the performance specifications, space applications also require that the MEMS structure sustains large accelerations during launch and detachment. For the sake of increasing the robustness of the structures, the designs included both the conventional in-plane mechanical stoppers at 2.9µm (full gap: 3µm) as well as cantilever-like ones at 2.8µm to gradually absorb impact (Figure 1). Additionally, out-of-plane displacement stoppers were implemented by fabricating encapsulation structures.

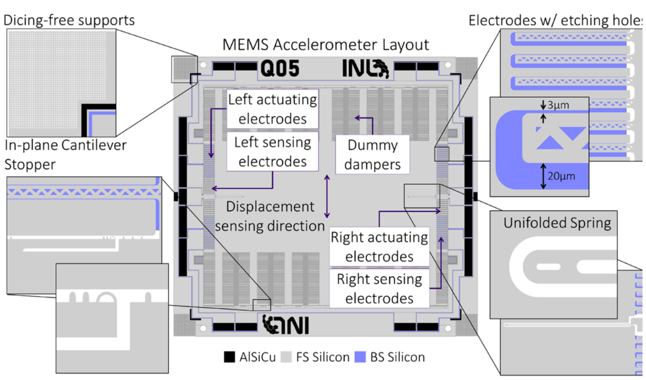

Figure 1. Designed and fabricated MEMS device (total die size: 13mm by 14mm).

Table 1. Microstructure's theoretical design parameters

Parameters	**S1**	**S2**
Mass, m [mg]	170	
Resonance Freq., Fn [Hz]	21.15	
Spring stiffness, k [N/m]	3.00	
Initial gap, d_0 [μm]	3.00	
Damping coeff., b [$mN.s/m$]	45.2	11.3
Number of dampers	898	224
Quality factor, Q	0.5	2.0
Brownian Noise, a_n [$nm/s^2/\sqrt{Hz}$]	167.80	83.90
Pull-in Voltage, V_{PI} [V]	2.38	
Pull-in time sensitivity, [$ms/(um/s^2)$]	1.174	0.014

DEVICE MICROFABRICATION

The accelerometers were fabricated using a three-mask dicing free MEMS process on a 50µm-thick active layer SOI wafer, as presented in [5]. The main fabrication steps are depicted in Figure 2. The fabricated devices are shown in Figure 3.

(a) Wafer preparation: Initially, alignment marks are patterned on the wafer frontside – FS and backside – BS to ensure the alignment between the structures on both sides.
(b) Metal Layer: A thin layer of AlSiCu, 500 nm, is sputtered on the FS and patterned for the electrical contacts.
(c) FS and BS SiO2 layer deposition: A 3 µm layer of silicon dioxide (SiO2) is deposited on both sides of the SOI wafer by plasma-enhanced chemical vapour deposition (PECVD).
(d) FS and BS Hard-mask patterning: The BS and FS oxide layers are then patterned by a reactive ion etching (RIE), to define the hard-masks for the subsequent silicon deep reactive ion etching (DRIE) step.
(e) FS and BS DRIE: The front and back sides are consecutively etched through DRIE, using the buried oxide as etch stop.
(f) Device release: The structures are finally released using hydrogen fluoride (HF) vapor etching.

Two different caps, serving as out-of-plane displacement stoppers, have been fabricated: one for the device bottom part that must accommodate the out-of-plane displacement due to earth gravity (not present in the final application, but necessary to be considered during the device characterization); and, a top side cap that limits the upper device displacement, preventing the collision

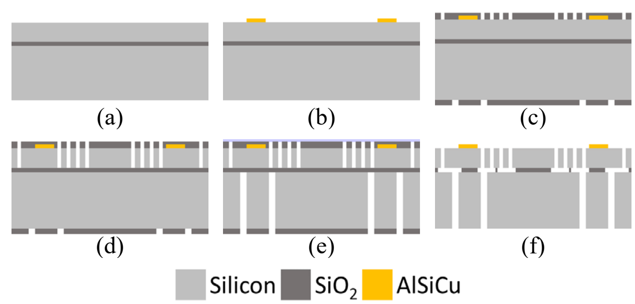

Figure 2: Accelerometer SOI-based fabrication process.

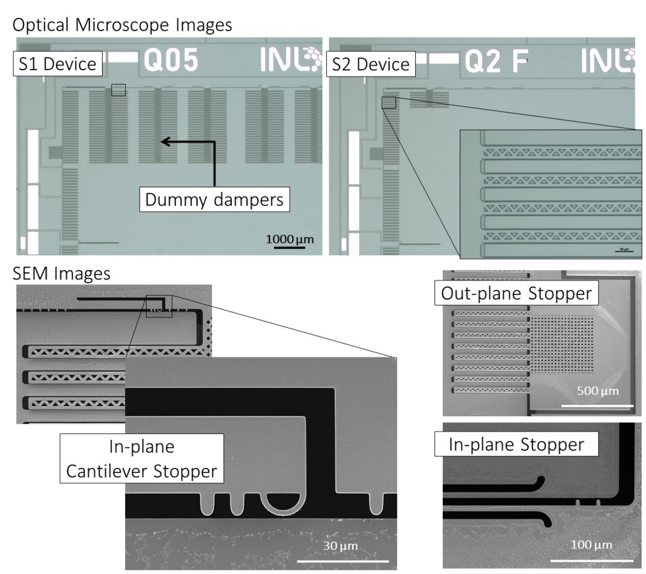

Figure 3. Designed and fabricated MEMS device (total die size: 13mm by 14mm).

of movable mass with the dummy dampers in the device layer. These caps were fabricated using a three-mask standard process on a SSP (Single Side Polished) wafer. The main fabrication steps are presented in Figure 4.

(a) FS and BS SiO2 layer deposition: a 3 µm and 5 µm layer of SiO2 is deposited on the FS and BS of the SSP wafer by PECVD.
(b) FS and BS hard-mask patterning: On the FS, a sequential SiO2 patterning is performed by two different lithography steps and by RIE process to create the multilevel hard-mask.
(c) The BS hard-mask is also patterned by RIE. The FS multilevel mask creates the cavity for the bottom caps and the top stoppers/pillars.
(d) FS 1st DRIE: The front side is initially etched through DRIE to a depth of 19um.
(e) FS hard-mask thinning DRIE: The FS SiO2 hard-mask is thinned by RIE until the thinner level is wholly removed.
(f) FS 2nd DRIE: Then, the front side Si is etched again. So the previously etched areas ended with 20um depth and the top stoppers with 1um.
(g) BS DRIE and cap release: Finally, the caps are etched by the BS through DRIE until the FS is reached and the caps are released from the wafer.

Given the large mass and the highly compliant springs, the resultant out-of-plane displacement is significant (around 10 µm as a result of the Earth's gravity). Therefore, these bottom and top caps are essential to ensure that the device does not get damaged or even break in the handling process and experimental testing. Closed top and bottom caps are also required for MEMS encapsulation.

The fabricated caps limit the out-of-plane displacement of the proof-mas to 20 µm in the negative z/down direction and 1 µm in the positive z/upper direction. This 1 µm limitation is fundamental as it prevents the movable mass (that includes handle layer silicon with a nominal gap of 2um defined but the BOX layer) from colliding with the dummy dampers. The encapsulation scheme and the final device are depicted in Figure 5.

EXPERIMENTAL RESULTS

Experimental Setup

The experimental setup used to evaluate the fabricated microstructures (1) comprises a charge amplifier circuit for capacitive displacement readout (2) and a data acquisition board for the readout voltage acquisition and actuation signal generation, mounted on a high-resolution 6-axis stage from ThorLabs (3), as displayed in Figure 6. The setup is fixed to an anti-vibration table (4) to minimize surrounding vibrations/noise interference.

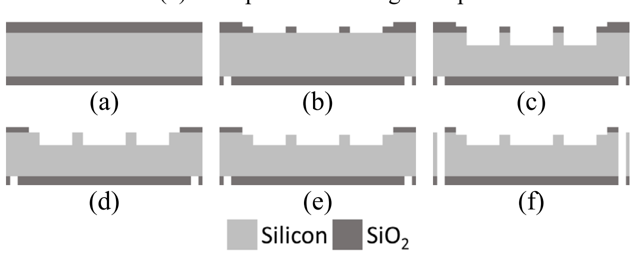

Figure 4. Out-plane stopper cap fabrication process.

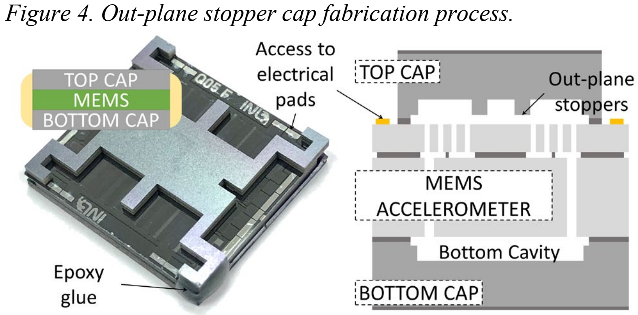

Figure 5. Device encapsulation (top and bottom caps).

Initially, with this high-resolution stage, it is possible to balance the structure to the rest position by correcting the tilt (that results from assembling the MEMS with the caps and its placement in the carrier). The external accelerations are induced in the accelerometer (acc_{ext}) by the tilting of the MEMS structure in the sensing direction, being null when the device is in its rest position and equal to the gravitational acceleration component along the device's sensing axis (acc_g). The proof-mass displacement will affect the gap of the sensing electrodes and with a capacitance to voltage readout circuit it's possible to electrically measure the external acceleration.

In parallel to the microstructure design and fabrication, a low noise electronic readout circuit was also pursued – given the low frequencies targeted, it becomes critical to reduce 1/f noise sources.

Performance Analysis

1) Mechanical features analysis:

Both devices (S1 and S2) were experimentally characterized for natural frequency (Fn), and quality factor. These features depend directly to the MEMS devices mechanical properties, such as mass, spring constant and damping coefficient, which in turn depend on layout and microfabrication parameters such as over-etch and notch. Both devices were evaluated by SEM inspection. The fabricated devices showed a silicon over-etch smaller than expected on the backside and in the electrodes regions, resulting in a larger proof-mass and a higher damping coefficient (smaller gap in the dampers). The springs' cross-section presented a trapezoidal shape, having a larger width in the device layer top surface and smaller in the near-BOX surface, which should translate to a lower stiffness. This resulted in lower Fn and Q, as depicted in the experimental measurements from Figure 7. Devices parameters extracted from measurements are detailed in Table 2. Furthermore, the nominal pull-in voltage of both devices was also experimentally characterized and is also presented in Figure 7.

2) Pull-in voltage sensitivity:

Given the mechanical properties achieved in device S2, this was used to validate pull-in operation. The pull-in voltage was measured for several external accelerations, resulting in the pull-in voltage sensitivity of 218 V/g, presented in Figure 8.

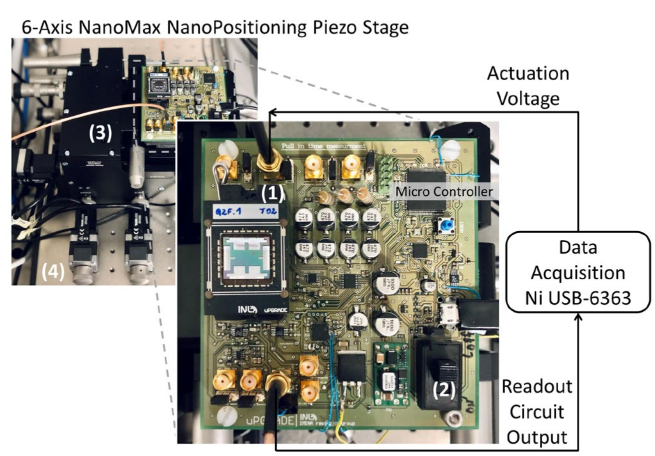

Figure 6. Experimental setup for device characterization.

CONCLUSIONS

A MEMS accelerometer based on pull-in time transduction is presented for geodetic applications. The devices were fabricated through a dicing-free standard SOI-based process, using 50 µm-thick device layer. Furthermore, to ensure the yield of the devices, encapsulation structures were also fabricated. The proposed designs show a large proof-mass (170 mg) with dummy parallel-plates patterned in the device layer to significantly increase the damping coefficient, critical in pull-in-based accelerometers. This approach has been analyzed and implemented using two different designs, differing in the number of dampers and resulting quality factor (device S1 with a theoretical Q factor of 0.5 and S2 with 2). The fabricated devices were experimentally characterized to determine the actual mechanical features and the device behaviour. A silicon over-etch smaller than expected was observed, resulting in smaller electrodes' and dampers' gaps, and a Q-factor of 0.36 and 0.65 were characterized for the devices S1 and S2, respectively. Furthermore, the pull-in voltage of the device S2 was characterized since this was the device that presented the damping coefficient in the desired region, and a pull-in voltage sensitivity of 218 V/g was measured.

The pull-in time sensitivity measurement is currently being pursued since this is a key performance parameter. The high sensitivities expected for these accelerometers may position them as good candidates for the realization of high-performance MEMS geodetic-grade accelerometers. Noise performance and long-term stability are also currently under investigation.

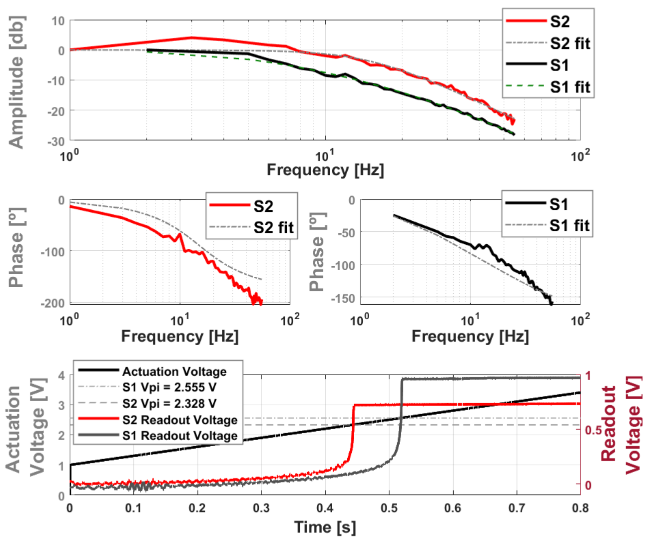

Figure 7: Experimental preliminary characterization of a fabricated S2 device.

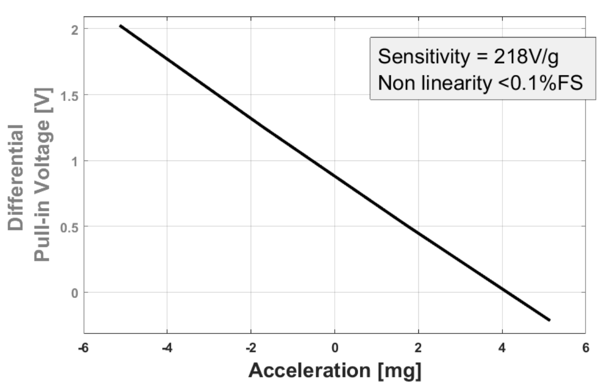

Figure 8: S2 differential pull-in voltage sensitivity, 218 [V/g].

Table 2. Microstructure's experimental parameters

Parameters	**S1**	**S2**
Mass, m [mg]	174	177
Resonance Freq., Fn [Hz]	11.8	14.9
Spring stiffness, k [N/m]	2.64	
Initial gap, $d0$ [μm]	2.2	
Damping coeff., b [$mN.s/m$]	94.3	24.1
Number of dampers	898	224
Quality factor, Q	0.36	0.65
Pull-in Voltage, V_{PI} [V]	2.56	2.33

ACKNOWLEDGMENTS

These developments have been carried out under the project uPGRADE - Miniaturized Prototype for Gravity field Assessment using Distributed Earth-orbiting assets (reference POCI-01-0247-FEDER-045927), co-funded by COMPETE 2020 - Operational Programme for Competitiveness and Internationalization under the PORTUGAL 2020 Partnership Agreement, through the European Regional Development Fund (ERDF), and by the Portuguese Foundation for Science and Technology (FCT) under the UT Austin Portugal Program.

REFERENCES

[1] B. D. Tapley, "GRACE Measurements of Mass Variability in the Earth System," *Science (1979)*, vol. 305, no. 5683, pp. 503–505, 2004, doi: 10.1126/science.1099192.

[2] B. Christophe *et al.*, "A new generation of ultra-sensitive electrostatic accelerometers for GRACE Follow-on and towards the next generation gravity missions," *Acta Astronautica*, vol. 117, no. September 2010, pp. 1–7, 2015, doi: 10.1016/j.actaastro.2015.06.021.

[3] W. T. Pike, I. M. Standley, S. B. Calcutt, and A. G. Mukherjee, "A broad-band silicon microseismometer with 0.25 NG/rtHz performance," in *Proceedings of the IEEE International Conference on Micro Electro Mechanical Systems (MEMS)*, 2018, vol. 2018-January. doi: 10.1109/MEMSYS.2018.8346496.

[4] R. P. Middlemiss, A. Samarelli, D. J. Paul, J. Hough, S. Rowan, and G. D. Hammond, "Measurement of the Earth tides with a MEMS gravimeter," *Nature*, vol. 531, no. 7596, 2016, doi: 10.1038/nature17397.

[5] I. S. Garcia, E. E. Moreira, R. A. Dias, J. Gaspar, F. S. Alves, and L. A. Rocha, "Sub-Micron Mems Accelerometer with Handle-Layer Patterning for Damping Enhancement Using Time Transduction," in *2019 20th International Conference on Solid-State Sensors, Actuators and Microsystems and Eurosensors XXXIII, TRANSDUCERS 2019 and EUROSENSORS XXXIII*, 2019, pp. 2045–2048. doi: 10.1109/TRANSDUCERS.2019.8808247.

[6] R. A. Dias *et al.*, "Real-Time Operation and Characterization of a High-Performance Time-Based Accelerometer," *Journal of Microelectromechanical Systems*, 2015, doi: 10.1109/JMEMS.2015.2487686.

CONTACT

*Rosana A. Dias; rosana.dias@inl.int.